Coherent phonons in pyrochlore titanates $A_2Ti_2O_7$ (A = Dy, Gd, Tb): A phase transition in $Dy_2Ti_2O_7$ at 110 K

N. Kamaraju,[1] Sunil Kumar,[1] Surajit Saha,[1] Surjeet Singh,[2] R. Suryanarayanan,[2] A. Revcolevschi,[2] and A. K. Sood[1]

[1]*Department of Physics and Center for Ultrafast Laser Applications (CULA), Indian Institute of Science, Bangalore - 560 012, India*

[2]*Laboratoire de Physico-Chimie de l'Etat Solide, ICMMO, CNRS, UMR8182, Btiment 414, Université Paris-Sud, FR-91405 Orsay, France*

(Received 7 October 2010; revised manuscript received 2 March 2011; published 5 April 2011)

We study the generation of coherent optical phonons in spin-frustrated pyrochlore single crystals $Dy_2Ti_2O_7$, $Gd_2Ti_2O_7$, and $Tb_2Ti_2O_7$ using femtosecond laser pulses (65 fs, 1.57 eV) in degenerate time-resolved transmission experiments as a function of temperature from 4 to 296 K. At 4 K, two coherent phonons are observed at ~5.3 THz (5.0 THz) and ~9.3 THz (9.4 THz) for $Dy_2Ti_2O_7$ ($Gd_2Ti_2O_7$), whereas three coherent phonons are generated at ~5.0, 8.6, and 9.7 THz for $Tb_2Ti_2O_7$. In the case of spin-ice $Dy_2Ti_2O_7$, a clear discontinuity is observed in the linewidths of both the coherent phonons as well as in the phase of lower-energy coherent phonon mode, indicating a subtle structural change at 110 K. Another important observation is a phase difference of π between the modes in all the samples, thus suggesting that the driving forces behind the generation of these modes could be different in nature, unlike a purely impulsive or displacive mechanism.

DOI: 10.1103/PhysRevB.83.134104 PACS number(s): 78.47.J−, 63.70.+h, 61.50.Ks, 63.20.kg

I. INTRODUCTION

Geometrically frustrated magnetic systems are the ones in which spins can not simultaneously satisfy all of their pair-wise exchange interactions due to geometrical reasons and, hence, not find a unique ground state.[1,2] In a real system, however, any small perturbation to these interactions can favor a particular ground state, thus lifting the macroscopic degeneracy. The perturbation can be in the form of single-ion anisotropy, next- or higher-neighbor interactions, thermal or quantum fluctuations, dipolar interactions, lattice deformations, or externally applied stimuli such as pressure or magnetic field. The rare-earth pyrochlore titanates with stoichiometry $A_2Ti_2O_7$ (A = Sm, Gd, Tb, Dy, Ho, ...) are typical examples of geometrically frustrated magnets in three dimensions.

There have been a few detailed Raman studies on these pyrochlores as a function of pressure[3,4] and temperature.[4–7] A subtle phase transition at $\Im_c \sim 110$ K was indicated for the spin-ice compound $Dy_2Ti_2O_7$ by Saha *et al.*[5] by the appearance of an extra Raman mode (~297 cm^{-1}) below $\Im_c$, which redshifts to 285 cm^{-1} at 12 K. This subtle phase transition was supported by their x-ray studies with an abrupt jump in the lattice parameter at ~110 K. No such changes are seen in nonmagnetic pyrochlore $Lu_2Ti_2O_7$. Nuclear gamma resonance of $^{161}Dy^{3+}$ in $Dy_2Ti_2O_7$ by Mössbauer spectroscopy[8] also suggested a change in the nuclear quadrupolar interaction with temperature. A significant change in the electric field gradient of $4f$ orbitals was seen with temperature, becoming zero at ~110 K. This led to the proposal[5] that, when the electric field gradient at Dy^{3+} ions due to their $4f$ orbitals becomes negligibly small, the surrounding atoms in the lattice possibly readjust slightly and move out of their regular Wyckoff positions, thus deforming the local symmetry but without disturbing the average electric field gradient due to the surrounding ions in the lattice.

Degenerate femtosecond time-resolved transmission and reflection experiments have been used to generate and explore the nature of coherent phonons in real time. The generation of coherent phonons makes it possible to have an insight into the microscopic nature of the laser-controlled atomic motion.[9] The ability to drive and control coherent lattice vibrations through an external impulsive femtosecond light pulse opens up many exciting possibilities, which include nonthermal melting,[10] insulator-to-metallic phase transitions,[11] paraelectric to ferroelectric transitions,[12] and selective opening of the caps of the nanotubes.[13] These experiments have prompted the development of many theories to explain the generation mechanism of the coherent phonons. For example, impulsive stimulated Raman scattering (ISRS) was proposed for the generation of coherent phonons in transparent materials,[14] whereas displacive excitation of coherent phonons (DECP) was proposed for opaque samples.[15,16] Later, it was shown that, by including both virtual and real transitions, ISRS (Refs. 17–19) could completely account for the generation of coherent phonons in opaque samples too. In fact, it was established that ISRS under resonant excitations and DECP are the same.[17,19] All these proposals describe the equation of motion for the relevant coherent phonon mode's normal coordinate Q as a driven damped harmonic oscillator

$$\frac{d^2Q}{dt^2} + \frac{1}{\tau}\frac{dQ}{dt} + \Omega_0^2 Q = F(t). \tag{1}$$

Here, $\Omega_0/2\pi$ is the natural frequency (ν_0) of the oscillator and τ is the phonon lifetime. Under the assumption that the dielectric function $\varepsilon(\omega) \equiv \varepsilon_1(\omega) + i\varepsilon_2(\omega)$ is a slowly varying function within the spectral width of the pump pulse, the Fourier component of the driving force $F(t)$ is given by[19]

$$F(\Omega) = A\left(\frac{d[\varepsilon_1(\omega)]}{d\omega} + \frac{2i\varepsilon_2(\omega)}{\Omega}\right) I(\Omega), \tag{2}$$

where A is a constant and both $\frac{d[\varepsilon_1(\omega)]}{d\omega}$ and $\varepsilon_2(\omega)$ are evaluated at the central frequency ω_L of the laser pulse. I(Ω) is the Fourier transform of the laser pulse intensity $I(t)$. The first term in Eq. (2) is the contribution from the virtual transitions, while the second term is the contribution from the real transitions

(absorption) of the excited carriers. It has also been shown[19] that, when the first term in Eq. (2) dominates (transparent materials), the phonon coordinate is $Q \sim \sin(\Omega_0 t + \phi)$ with $\phi = 0$, whereas $Q \sim \sin(\Omega_0 t + \phi)$ with $\phi = \pi/2$ is expected in the case of dominant real transitions (opaque samples). Thus, determination of the initial phases of these modes can throw some insight on the generation mechanisms involved. When the driving force is a complex quantity[20] (both real and virtual transitions exist simultaneously), $Q \sim \sin(\Omega_0 t + \phi)$, where ϕ can take on any values between 0 and 2π. The phonon phase as a fingerprint in structural phase transitions has not been explored so far.

There have been no reports of coherent phonons in the pyrochlore systems until now. Here, we present the results of degenerate time-resolved transmission experiments with femtosecond pulses (~65 fs time duration and central photon energy of 1.57 eV) for $Dy_2Ti_2O_7$, $Gd_2Ti_2O_7$, and $Tb_2Ti_2O_7$ as a function of temperature from 296 down to 4 K. At the lowest temperature of 4 K, two coherent phonons at ~5.3 THz (5.0 THz) and ~9.3 THz (9.4 THz) are observed for $Dy_2Ti_2O_7$ ($Gd_2Ti_2O_7$), whereas three coherent phonon modes at ~5.0, 8.6, and 9.7 THz are observed for $Tb_2Ti_2O_7$. In the case of coherent phonons in $Dy_2Ti_2O_7$, a clear discontinuity in the linewidths of both the coherent phonon modes and the phase ϕ of the low-energy coherent phonon mode at $\Im_C \sim 110$ K are seen, confirming a subtle structural change at $\Im_C$. Another important observation is the phase difference of π between the modes in all the samples. The initial phase of π for the modes suggests that the driving force is a mixture of purely impulsive and displacive parts,[20] as compared to the initial phase zero of a purely impulsive mechanism. We also compare the results of the coherent phonons with the Raman results.

II. SYSTEMS STUDIED

Preparation and characterization of the single crystals of the pyrochlore titanates used in this work were described before.[3–5] Thin circular slices of ⟨111⟩ cut single crystals (diameter of 3 mm and thickness of 0.5 mm) were used in our experiments.

A pyrochlore compound crystallizes into a face-centered-cubic lattice with the space group $Fd\bar{3}m$ (O_7^h) with two formula units in a primitive cell. It has four distinct and nonequivalent sites, namely, A, B, O, and O′ and, hence, also represented as $A_2B_2O_6O'$. Since there are two formula units of $A_2B_2O_7$ in a pyrochlore unit cell, there are totally 66 normal modes of vibration, out of which only six ($A_{1g} + E_g + 4F_{2g}$) are Raman active and seven ($7F_{1u}$) are infrared active modes. Although the assignment of the modes in literature has been consistent,[3–7,21–25] the reported data show all the Raman modes in both parallel and cross polarizations, even with varying angle of incidence,[7,22] thus indicating that pyrochlores do not fully comply with the group-theoretical selection rules. There remains an ambiguity in the assignment of some of the modes,[4] which will be discussed when we present our results.

III. EXPERIMENTAL TECHNIQUES

The degenerate pump-probe (PP) measurements were performed using laser pulses of ~50 fs duration [full width at half maximum (FWHM)] obtained from Ti:sapphire regenerative amplifier system (Spitfire Pro, Spectra Physics) operating at the central laser energy of 1.57 eV and repetition rate of 1 kHz. At the sample point, the cross correlation of pump and probe pulses was measured to be 65 fs (FWHM) using a thin BBO crystal. The pump pulse was delayed in time using the computer-controlled motorized translation stage (XPS Motion controller, Newport). The change in the probe transmission due to the presence of the pump was monitored using two Si-PIN diodes (one for the reference beam and the other for the probe beam interacting with the pump) with the standard lock-in detection (pump beam was chopped at 389 Hz). The probe fluence was kept at 50 μJ/cm^2 and the pump fluence was fixed at 3 mJ/cm^2. The spot sizes (half width at $1/e$ maximum) of the pump and probe beams were kept at 600 and 400 μm at the overlap of the two beams on the sample. All these measurements were performed with pump and probe polarizations perpendicular to each other to avoid pump beam scattering into the detector. Temperature-dependent studies were performed with the help of optical continuous-flow liquid-helium cryostat (MicrostatHe, Oxford Instruments) having optical windows operated at the temperature range of 4–296 K. Details of Raman measurements are given in Ref. 5.

IV. RESULTS AND DISCUSSIONS

A. Coherent phonons in $Dy_2Ti_2O_7$

Figure 1(a) displays normalized change in the time-resolved transmission $\frac{\Delta T}{T}$ of the probe beam after excitation with a pump pulse for $Dy_2Ti_2O_7$ at a few temperatures as a function of the pump-probe delay time (t). Here, ΔT is the change in transmission of the probe due to the presence of the pump and T is the transmission of the probe in the absence of the pump pulse. The data contain three parts: (i) a dip at pump-probe delay time $t = 0$ related to coherent artifact peak[26,27] that has a maximum value at the cross-correlation maximum, thus helping in the determination of exact origin of time delay ($t = 0$); (ii) nonoscillatory electronic background; and (iii) oscillatory signal associated with the coherent phonons. To extract the oscillatory part,[28] we have numerically differentiated $\frac{\Delta T}{T}$ data and fitted (from $t \sim 180$ fs after cutting the coherent artifact) with the following function:

$$\frac{d\left(\frac{\Delta T}{T}\right)}{dt} = \frac{d}{dt}\left(\sum_{i=1,2} B_i \exp(-t/\tau_i)\sin(2\pi\nu_i t + \phi_i)\right), \quad (3)$$

where B_i, τ_i, ν_i, and ϕ_i are the amplitude, lifetime, frequency, and phase of the coherent phonons. Numerically differentiated data and the fit are displayed in Fig. 1(b). The fast Fourier transform (FFT) of the oscillatory part of the data and the fit are shown in Fig. 1(c), where the y axis in the frequency range of 3–7 THz is scaled up appropriately. It can be seen that the first coherent phonon near ~5.3 THz is damped more and blue shifts as the temperature is increased and vanishes at 296 K. The two coherent modes seen in FFT spectra at 4 K [CP1: 5.3 THz and CP2: 9.3 THz in Fig. 1(c)] are the modes labeled as M3 and M6 in Raman spectra in Fig. 1 of Ref. 5. Following Refs. 3–7 and 21–25, the assignment of CP2 is F_{2g}, involving only 48f oxygen atoms. However, the assignment of CP1 is still being debated.[4–6] Earlier,[5–7,21–25]

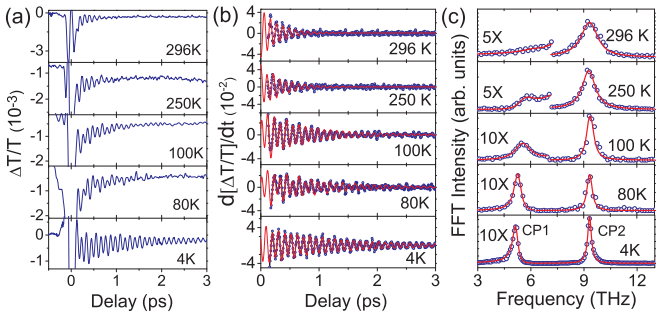

FIG. 1. (Color online) (a) As-recorded time-resolved transmission data of $Dy_2Ti_2O_7$ at various temperatures. (b) Time derivative of the data along with the fit as discussed in the text. (c) The corresponding FFT of the data and the fits.

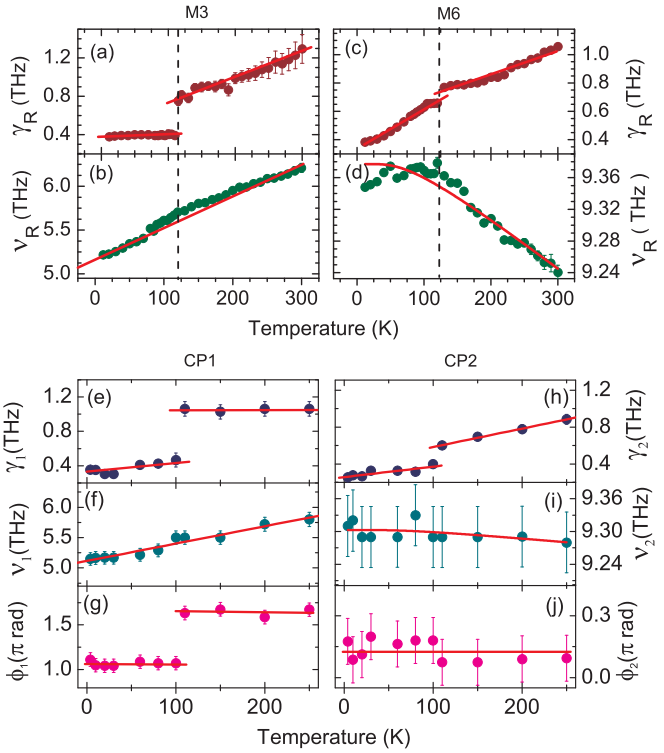

FIG. 2. (Color online) (a)–(d) Lorentzian fit parameters for M3 and M6 (γ_R and ν_R) vs sample temperature from the Raman spectra of Ref. 5 (see text). (e)–(j) Fit parameters for CP1 and CP2 vs temperature. The solid lines in panels (d) and (i) are anharmonic fits to the data (see text). In panels (a)–(c), (e), (f), and (h), solid lines are fits to linear functions to serve as a guide to the eye. In panels (g) and (j), solid lines are drawn as a guide to the eyes.

it was assigned to be a F_{2g} mode involving only vibrations of oxygen atoms at $8b$ sites that occupy the center of Dy_4 tetrahedron. Our recent studies on O^{18} substituted $Dy_2Ti_2O_7$ show[29] that this mode redshifts by only $\sim$1% as compared to the expected value of 5% seen for other modes.[5] Comparing the frequency of the mode in various pyrochlore titanates, the CP1 mode is assigned to disorder-activated Raman mode associated with the vibrations of Ti^{4+}[4]. To the best of our knowledge, the generation of coherent phonons not associated with group theoretically allowed Raman modes has not been reported before. The Lorentzian fit parameters (full width at half maximum γ_R and frequency ν_R) from the Raman data[5] are plotted versus temperature for the mode M3 in Figs. 2(a) and 2(b) and mode M6 (filled circles) in Figs. 2(c) and 2(d). The fit parameters of the time-domain data are presented in Figs. 2(e)–2(g) for the coherent phonon mode CP1 and in Figs. 2(h)–2(h) for the second coherent phonon mode CP2. It can be seen here that there is a clear jump in the linewidths $\gamma_{1,2}$ (full width at half maximum of the FFT spectra defined as $\frac{1}{\pi\tau_{1,2}}$, where $\tau_{1,2}$ is the phonon lifetime) of both the modes [Figs. 2(e) and 2(h)]. This behavior is consistent with the discontinuous change in Raman linewidths [see Figs. 2(a) and 2(c)] at $\sim$110 K for the corresponding modes M3 and M6 (dashed vertical line drawn at $\sim$110 K as a guide to the eye). As seen earlier[5] in Raman studies [Fig. 2(b)], the frequency of CP1 is anomalous [decrease in phonon frequency with decrease in temperature, see Fig. 2(f)] attributed to phonon-phonon anharmonic interactions. The thick lines in Fig. 2 are linear fits except for (d) and (i). The linewidths and frequencies are normally fitted with the well-known functions[30,31] based on cubic anharmonicity, where a phonon of frequency ν_0 decays into two phonons of equal frequency $\frac{\nu_0}{2}$:

$$\gamma(\Im) = \gamma_0 + C[1 + 2n(\nu_0/2)], \quad (4)$$

$$\nu(\Im) = \nu_0 + A[1 + 2n(\nu_0/2)], \quad (5)$$

where ν_0 (frequency at temperature $\Im = 0$), A, C, and γ_0 (disorder-induced linewidth) are the fitting parameters (A and C are the measures of third-order cubic anharmonicity), and $n(\nu_0/2)$ is the Bose-Einstein factor. We have fitted [thick line in Figs. 2(b) and 2(i)] the frequency of M6 and CP2 with Eq. (5). We note that the magnitude of change in linewidth of CP1 between 110 and 300 K [Fig. 2(e)] and frequency of CP2 between 4 and 300 K [Fig. 2(i)] are less as compared to the Raman counterparts [Figs. 2(a) and 2(d)]. The reason is not clear to us at present. We, however, note that the Raman parameters were obtained by fitting a sum of Lorentzians to a broad spectra comprising of many overlapping modes (see Fig. 2 of Ref. 5). This suggests that the temperature dependence of the linewidths extracted from present time-resolved studies is perhaps more reliable.

Next, we turn our attention to the phase ϕ of the coherent phonon modes. The phase ϕ_1 of CP1 is $\sim\pi$ at temperatures of 4–110 K, which changes abruptly to $\sim 1.6\pi$ after 110 K, whereas the phase ϕ_2 of CP2 remains at $\sim 0.1\pi$ throughout the whole temperature range [see Figs. 2(g) and 2(j)]. We recall that $\phi = 0$ for the spectrally integrated Stokes and $\phi = \pi$ for the anti-Stokes part of the probe spectrum.[18] The spectrally integrated probe spectrum (the present case) is observed to have a phase of zero,[28,32] resembling Stokes coherent phonons. In general, the initial phase could be influenced by factors such as thickness of the crystal, the electronic background subtraction, exact definition of the zero delay (maximum dip in the transmission data in our experiments),[20] and the finite pulse width of the laser approximately half of the phonon time period. All these factors can cause a systematic error in the measurement of phases, but still can not explain the π phase difference between the two modes. Since we numerically differentiate the data, the error in ϕ coming from the electronic background is avoided. Thus, in our experiments, the relevant source of error could be from the measurements in the time

step size of 6 fs, giving an error of ∼0.23 rad for CP1 and 0.38 rad for CP2. The phase difference $\Delta\phi$ of π between the two modes indicates that they are out of phase, perhaps suggesting a coupling between them. The sudden change in the phase occurs at 110 K, corroborating the changes in $\gamma_{1,2}$ arising from a subtle structural change. Moreover, the possible reason for observing the initial phase of π suggests that the driving force is complex for CP1 as compared to purely real force ($\phi = 0$) for CP2. It is noted that such phase difference of π between the two coherent phonon modes was observed in time-resolved reflectivity experiments on superconducting $YBa_2Cu_3O_{7-\delta}$ ($\delta < 0.1$) thin films,[33] but not explained. We do not yet understand the microscopic origin of the temperature dependence of the phases of the two coherent modes as well as the subtle phase transition at 110 K.

B. Coherent phonons in $Gd_2Ti_2O_7$

The time derivative of the differential transmission data (open circles) for a few temperatures is presented in Fig. 3(a) along with the fit (thick line) using Eq. (3). The corresponding FFT of the data and the fit are presented in Fig. 3(b), where the y axis in the lower frequency range of 3.5–7 THz is scaled up by six. The fit parameters from the time-domain data are given in Figs. 4(e)–4(g) for CP1 and in Figs. 4(h)–4(j) for CP2. The temperature dependence of linewidths and frequencies determined from as-recorded Raman spectra (data not shown) for M3 and M6 are displayed in Figs. 4(a) and 4(b) and 4(c) and 4(d), respectively. It can be seen that, in comparison to $Dy_2Ti_2O_7$, the coherent as well as Raman phonon parameters do not show any discontinuity or jump as the temperature is varied. The linewidths (of M3, M6, CP1, and CP2) and frequencies (of M6 and CP2) are fitted with the anharmonic model given by Eqs. (4) and (5) and the fit parameters to linewidth are given in Table I. More theoretical work is needed to understand the coherent generation of modes not predicted by selection rules. The temperature dependence of the frequency of CP1 [Fig. 4(f)] is anomalous, similar to its behavior in $Dy_2Ti_2O_7$ and other pyrochlore samples as observed in Raman studies,[3–7] and linear fits are drawn in Figs. 4(f) and 4(b). The variation of phases ϕ_1 and ϕ_2 is

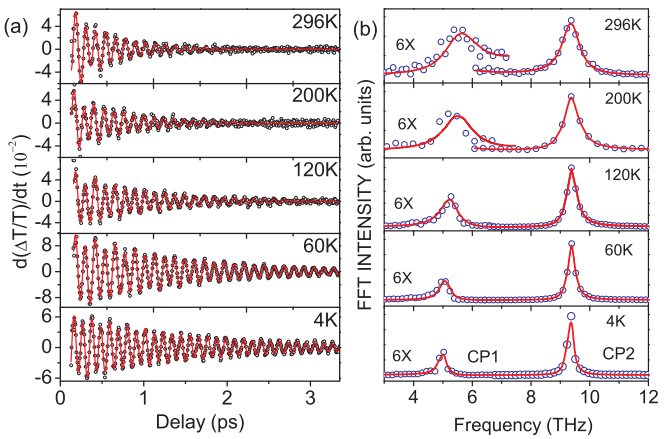

FIG. 3. (Color online) (a) Time derivative of the raw data along with the fit as discussed in the text for $Gd_2Ti_2O_7$. (b) The corresponding FFT of the data and the fits.

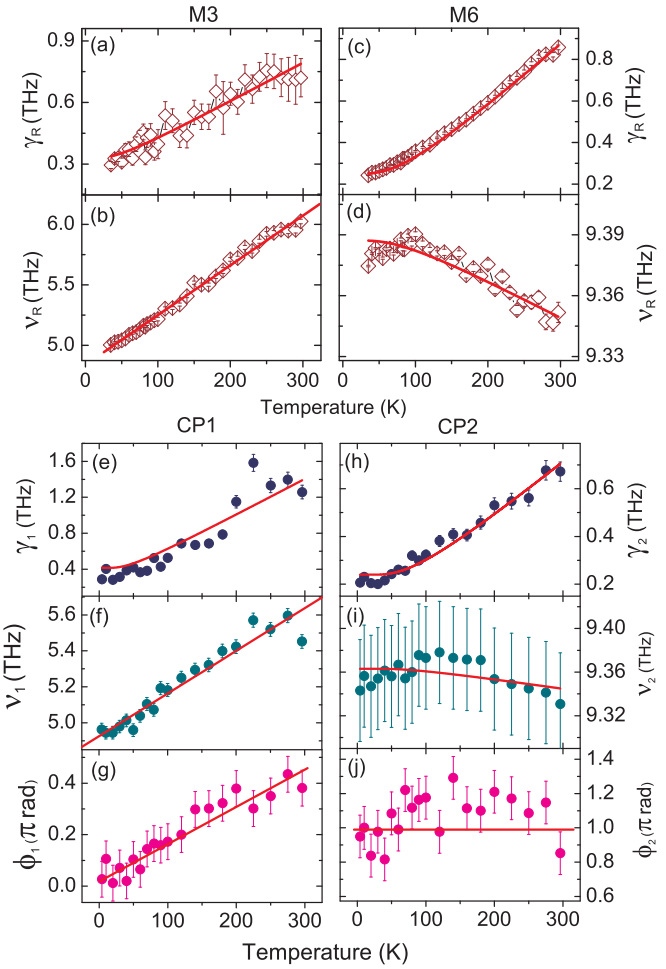

FIG. 4. (Color online) (a)–(d) Lorentzian fit parameters for M3 and M6 (γ_R and ν_R) vs sample temperature from Raman spectra of $Gd_2Ti_2O_7$. (e)–(j) Fit parameters for CP1 and CP2 vs temperature. The solid lines in panels (b), (f), and (g) are fits to linear functions. These, along with the solid line in panel (j), are drawn to serve as a guide to the eyes.

presented in Figs. 4(g) and 4(j) for modes CP1 and CP2, respectively. The phase difference of π between the two modes at 4 K indicates that the driving force is complex and the two modes are perchance coupled as found in $Dy_2Ti_2O_7$. However, it is surprising to see a systematic increase of the phase ϕ_1

TABLE I. The anharmonic fit parameters for $Gd_2Ti_2O_7$ and $Tb_2Ti_2O_7$.

Compound	Mode	ν_0 (THz)	γ_0 (THz)	C (THz)
$Gd_2Ti_2O_7$	M3	4.98	0.217	0.113
	CP1	4.84	0.20	0.23
	M6	9.38	0.025	0.32
	CP2	9.38	0.030	0.270
$Tb_2Ti_2O_7$	P1	5.20	0.006	0.37
	CP1	4.89	0.003	0.290
	P3	8.93	0.68	0.22
	CP2	8.55	0.20	0.45
	P5	9.63	0.64	0.17
	CP3	9.60	0.325	0.210

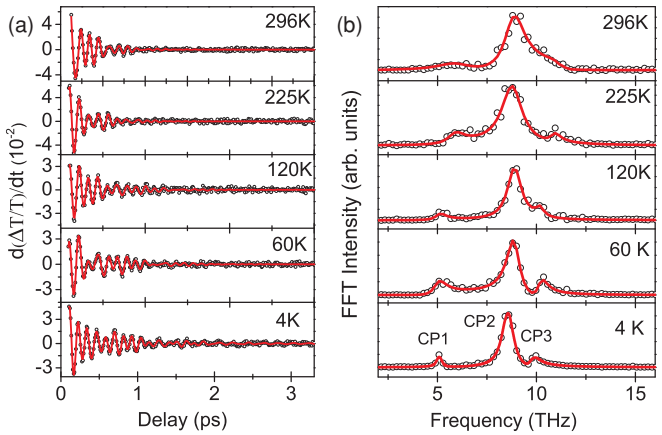

FIG. 5. (Color online) (a) Time derivative of the raw data along with the fit as discussed in the text for $Tb_2Ti_2O_7$. (b) The corresponding FFT of the data and the fits.

going from 0 at 4 K to π at 296 K (0.004 rad/K). This suggests that the driving force responsible for CP1 changes from purely real at 4 K to a complex quantity at 296 K. We do not understand the temperature dependence of ϕ_1. On the other hand, for CP2, the phase ϕ_2 is almost constant over the entire temperature range.

C. Coherent phonons in $Tb_2Ti_2O_7$

The numerical differentiation of normalized change in transmission data (open circles) for a few temperatures are presented in Fig. 5(a) along with the fit using the differentiation of the sum of the three damped harmonic oscillators (CP1, CP2, and CP3). The corresponding FFT of the data and the fit are presented in Fig. 5(b). The variation of the fitting parameters of the three modes (CP1, CP2, and CP3) from time-domain data as a function of temperature are presented in the left [Figs. 6(a2)–6(c2)], middle [Figs. 6(d2)–6(f2)], and right [Figs. 6(g2)–6(i2)] panels. The frequencies ($\nu_{i=1,2,3}$) of these three modes at 4 K are 5.0 THz (ν_1), 8.6 THz (ν_2), and 9.7 THz (ν_3). The temperature dependence of frequencies and linewidths of corresponding Raman modes labeled as P1, P3, and P4 in Fig. 1 of Ref. 4 are displayed in Figs. 6(a1)–6(e1) for comparison. The linewidths are fitted using the cubic anharmonic model [Eq. (4)] and the fit parameters are given in Table I. It can be seen from Table I that, similar to $Gd_2Ti_2O_7$, the disorder contribution to the linewidth is smaller for the coherent phonon modes compared to the corresponding Raman modes. The frequencies of all these modes are anomalous as also observed in Raman measurements[4,6] and, hence, a linear fit is shown [see Figs. 6(b1), 6(e1), 6(b2), 6(e2), and 6(h2)]. The difference in the temperature dependence of P4 and CP3 is not clear. CP1 exhibits π phase difference with respect to CP2 and CP3, indicating possible coupling between them: the phase ϕ_1 of CP1 is 0, whereas for the other two modes, $\phi_{2,3} \cong \pi$ throughout the whole sample temperature range [see Figs. 6(c2), 6(f2), and 6(i2)]. We note that the abrupt changes in the coherent phonon parameters seen for $Dy_2Ti_2O_7$ at 110 K are absent in those of $Tb_2Ti_2O_7$.

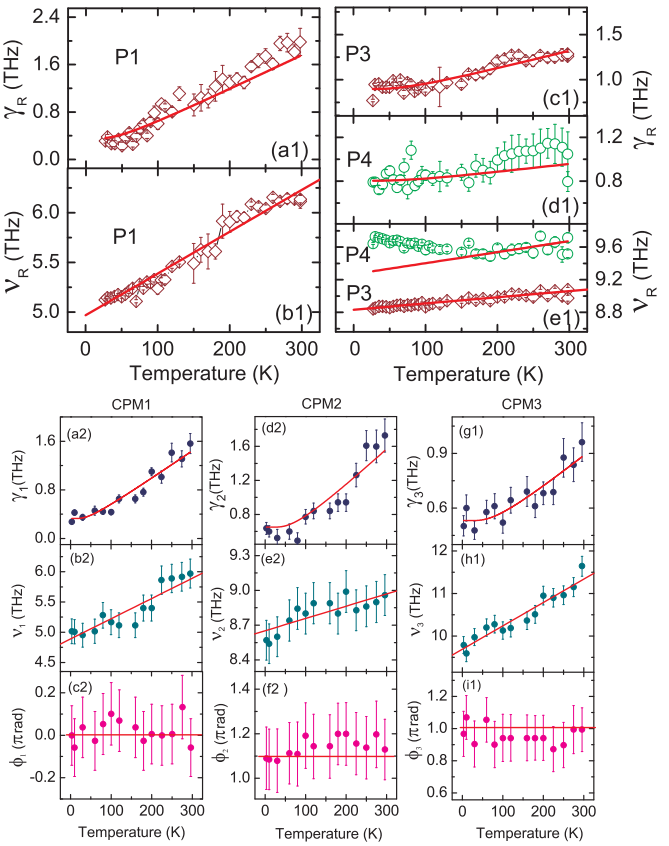

FIG. 6. (Color online) (a1)–(e1) Lorentzian fit parameters for P1, P3, and P4 (γ_R and ν_R) vs sample temperature from Raman spectra (Ref. 4) of $Tb_2Ti_2O_7$. (a2)–(i2) Fit parameters for CP1, CP2, and CP3 vs temperature for $Tb_2Ti_2O_7$. The solid lines in panels (a1), (c1), (d1), (a2), (d2), and (g1) are anharmonic fits to the data (see text). Solid lines in remaining panels are fits to linear functions to serve as a guide to the eyes.

V. CONCLUSIONS

In conclusion, we have carried out degenerate pump-probe transmission experiments to investigate coherent phonons of three pyrochlores, $Dy_2Ti_2O_7$, $Gd_2Ti_2O_7$, and $Tb_2Ti_2O_7$, as a function of temperature. In the case of $Dy_2Ti_2O_7$, a clear discontinuity is observed in the linewidths of both the coherent phonon modes as well as in the phase of the low-energy coherent phonon, indicating a subtle structural change at 110 K. In comparison, such changes are not seen in the coherent phonons of $Gd_2Ti_2O_7$ and $Tb_2Ti_2O_7$. Another notable observation is the phase difference of π between the modes in all the samples, thus suggesting that the driving forces behind the generation of these modes are different in nature, unlike a purely impulsive or displacive driving force. We hope that our observation of temperature dependence of the phase of phonons and relative phase difference between the modes will motivate further theoretical understanding of the femtosecond-controlled atomic motion. Further, the implications of a subtle phase transition at 110 K in $Dy_2Ti_2O_7$ toward the exotic physics of the spin-ice phase[34] at lower temperatures will be worth exploring.

ACKNOWLEDGMENTS

We thank the Indo-French Centre for Promotion of Advanced Research (IFCPAR) [Centre Franco-Indien pour la Promotion de la Recherche Avancée (CEFIPRA)] for financial support under Project No. 3108-1. A.K.S. acknowledges the Department of Science and Technology (DST), India, for financial support. S.K. acknowledges University Grants Commission (UGC) for financial support.

[1] A. P. Ramirez, Annu. Rev. Mater. Sci. **24**, 453 (1994).
[2] R. Moessner and A. P. Ramirez, Phys. Today **59**(2), 24 (2006).
[3] S. Saha, D. V. S. Muthu, C. Pascanut, N. Dragoe, R. Suryanarayanan, G. Dhalenne, A. Revcolevschi, S. Karmakar, S. M. Sharma, and A. K. Sood, Phys. Rev. B **74**, 064109 (2006).
[4] S. Saha, D. V. S. Muthu, S. Singh, B. Dkhil, R. Suryanarayanan, G. Dhalenne, H. K. Poswal, S. Karmakar, S. M. Sharma, A. Revcolevschi, and A. K. Sood, Phys. Rev. B **79**, 134112 (2009).
[5] S. Saha, S. Singh, B. Dkhil, S. Dhar, R. Suryanarayanan, G. Dhalenne, A. Revcolevschi, and A. K. Sood, Phys. Rev. B **78**, 214102 (2008).
[6] M. Mączka, M. L. Sanjuán, A. F. Fuentes, K. Hermanowicz, and J. Hanuza, Phys. Rev. B **78**, 134420 (2008).
[7] M. Mączka, M. L. Sanjuán, A. F. Fuentes, L. Macalik, J. Hanuza, K. Matsuhira, and Z. Hirori, Phys. Rev. B **79**, 214437 (2009).
[8] A. Almog, E. R. Bauminger, A. Levy, I. Nowik, and S. Ofer, Solid State Commun. **12**, 693 (1973).
[9] T. Garl, E. G. Gamaly, D. Boschetto, A. V. Rode, B. Luther-Davies, and A. Rousse, Phys. Rev. B **78**, 134302 (2008).
[10] A. Rousse, C. Rischel, S. Fourmaux, I. Uschmann, S. Sebban, G. Grillion, Ph. Balcou, E. Forster, J. P. Geindre, P. Audebert, J. C. Gauthier, and D. Hulin, Nature (London) **410**, 65 (2001).
[11] M. Chollet, L. Cuerin, N. Uchida, S. Fukaya, H. Shimoda, T. Ishikawa, K. Matsuda, T. Hasegawa, A. Ota, H. Yamochi, G. Saito, R. Tazaki, S. I. Adachi, and S.-Y. Koshihara, Science **307**, 86 (2005).
[12] E. Collet, M.-H. Lemee-Cailleau, M. B.-L. Cointe, H. Cailleau, M. Wulff, T. Luty, S.-Y. Koshihara, M. Meyer, L. Toupet, P. Rabiler, and S. Techert, Science **300**, 612 (2003).
[13] T. Dumitrica, M. E. Garcia, H. O. Jeschke, and B. I. Yakobson, Phys. Rev. Lett. **92**, 117401 (2004).
[14] L. Dhar, J. A. Rogers, and K. A. Nelson, Chem. Rev. (Washington, DC, US) **94**, 157 (1994).
[15] T. K. Cheng, J. Vidal, H. J. Zeiger, G. Dresselhaus, M. S. Dresselhaus, and E. P. Ippen, Appl. Phys. Lett. **59**, 1923 (1991).
[16] H. J. Zeiger, J. Vidal, T. K. Cheng, E. P. Ippen, G. Dresselhaus, and M. S. Dresselhaus, Phys. Rev. B **45**, 768 (1992).
[17] G. A. Garrett, T. F. Albrecht, J. F. Whitaker, and R. Merlin, Phys. Rev. Lett. **77**, 3661 (1996).
[18] R. Merlin, Solid State Commun. **102**, 207 (1997).
[19] T. E. Stevens, J. Kuhl, and R. Merlin, Phys. Rev. B **65**, 144304 (2002).
[20] A. V. Bragas, C. Aku-Leh, S. Costantino, A. Ingale, J. Zhao, and R. Merlin, Phys. Rev. B **69**, 205306 (2004).
[21] M. T. Vandenborre, E. Husson, J. P. Chatry, and D. Michel, J. Raman Spectrosc. **14**, 63 (1983).
[22] T. T. A. Lummen, I. P. Handayani, M. C. Donker, D. Fausti, G. Dhalenne, P. Berthet, A. Revcolevschi, and P. H. M. van Loosdrecht, Phys. Rev. B **77**, 214310 (2008).
[23] M. Mączka, J. Hanuza, K. Hermanowicz, A. F. Fuentes, K. Matsuhira, and Z. Hiroi, J. Raman Spectrosc. **39**, 537 (2008).
[24] F. X. Zhang and S. K. Saxena, Chem. Phys. Lett. **413**, 248 (2005).
[25] N. J. Hess, B. D. Begg, S. D. Conradson, D. E. McCready, P. L. Gassman, and W. J. Weber, J. Phys. Chem. B **106**, 4663 (2002).
[26] J. K. Wahlstrand and R. Merlin, Phys. Rev. B **68**, 054301 (2003).
[27] J. Swiatkiewicz, P. N. Prasad, and B. A. Reinhardt, Opt. Commun. **157**, 135 (1998).
[28] P. Němec and P. Maly, Phys. Rev. B **72**, 235324 (2005).
[29] S. Saha, S. Singh, R. Suryanarayanan, A. Revcolevschi, and A. K. Sood (unpublished).
[30] M. Balkanski, R. F. Wallis, and E. Haro, Phys. Rev. B **28**, 1928 (1983).
[31] J. Menéndez and M. Cardona, Phys. Rev. B **29**, 2051 (1984).
[32] Y. S. Lim, S.-C. Yoon, K.-J. Yee, J.-H. Lee, D. S. Kim, and D. Lee, Phys. Rev. B **68**, 153308 (2003).
[33] W. Albrecht, T. Kruse, and H. Kurz, Phys. Rev. Lett. **69**, 1451 (1992).
[34] A. P. Ramirez, A. Hayashi, R. J. Cava, R. Siddharthan, and B. S. Shastry, Nature (London) **399**, 333 (1999).